Article

Surface Functionalization of Iron Oxide Nanoparticles with Gallic Acid as Potential Antioxidant and Antimicrobial Agents

Syed Tawab Shah [1], Wageeh A. Yehye [1,*], Omar Saad [2], Khanom Simarani [3], Zaira Zaman Chowdhury [1,*], Abeer A. Alhadi [2] and Lina A. Al-Ani [1]

[1] Nanotechnology & Catalysis Research Centre (NANOCAT), University of Malaya, Block A, Level 3, Institute of Postgraduate Studies Building, Kuala Lumpur 50603, Malaysia; tawab_shah2003@yahoo.com (S.T.S.); linaalani@ymail.com (L.A.A.-A.)

[2] Department of Pharmacy, Faculty of Medicine, University of Malaya, Kuala Lumpur 50603, Malaysia; omar79@siswa.um.edu.my (O.S.), abeer@um.edu.my (A.A.A.)

[3] Institute of Biological Sciences, Faculty of Science, University of Malaya, Kuala Lumpur 50603, Malaysia; hanom_ss@um.edu.my (K.S.)

* Correspondence: wdabdoub@um.edu.my (W.A.Y.); dr.zaira.chowdhury@um.edu.my (Z.Z.C.); Tel.: +60-3-7967-2924 (W.A.Y.); +60-3-7967-6954 (Z.Z.C.); Fax: +60-3-7967-6956 (W.A.Y.); +60-3-7967-6556 (Z.Z.C.).

Abstract: In this research, we report the size-controlled synthesis and surface-functionalization of magnetite with the natural antioxidant gallic acid (GA) as a ligand, using in situ and post-synthesis methods. GA functionalization provided narrow size distribution, with an average particle size of 5 and 8 nm for in situ synthesis of gallic acid functionalized magnetite IONP@GA1 and IONP@GA2, respectively, which are ultra-small particles as compared to unfunctionalized magnetite (IONP) and post functionalized magnetite IONP@GA3 with average size of 10 and 11 nm respectively. All the IONPs@GA samples were found hydrophilic with stable aggregation state. Prior to commencement of experimental lab work, PASS software was used to predict the biological activities of GA and it is found that experimental antioxidant activity using 2,2-diphenyl-1-picrylhydrazyl (DPPH) assay and antimicrobial studies using well diffusion method are in good agreement with the simulated results. Furthermore, the half maximal inhibitory concentration (IC50) values of DPPH antioxidant assay revealed a 2–4 fold decrease as compared to unfunctionalized IONP. In addition to antioxidant activity, all the three IONP@GA proved outstanding antimicrobial activity while testing on different bacterial and fungal strains. The results collectively indicate the successful fabrication of novel antioxidant, antimicrobial IONP@GA composite, which are magnetically separable, efficient, and low cost, with potential applications in polymers, cosmetics, and biomedical and food industries.

Keywords: gallic acid; nanoantioxidant; DPPH; functionalization; antimicrobial

---

1. Introduction

The role of antioxidants in maintaining healthy cells status is well-defined, with a very large amount of research and published articles [1–5]. The endogenous antioxidant defense system is usually sufficient in handling free radicals in the body, while in disease developing-threshold circumstances, the critical need for exogenous antioxidants rises [5].

The fast-growing field of nanotechnology has recently presented a remarkable resolution that can even surpass exogenous dietary antioxidant sources [5]. Nanoantioxidants constitute the upcoming antioxidant agents for therapeutic and industrial applications [6]. Their powerful activity is believed to present more effective dominance over various Reactive Oxygen Species (ROS) [6].

Of late, researchers have investigated antioxidant activity of various metal-based nanocomposites, such as gold [7,8], platinum [9–11], iron [12–14], nickel oxide [15], ceria [16,17], and yttria [2,18], for applications as nanoantioxidants. Magnetic IONPs owe protuberant antioxidant activity against oxidative damage-related diseases [19–25]. However, there are several factors that strongly affect nanomaterials antioxidant activity for instance chemical composition, surface charge, particle size, and coating of the surface [6,26–29]. The surface coating could be biocompatible, nontoxic and allow targeted drug delivery [30–35].

Gallic acid (GA) is a well-known powerful natural antioxidant constituent of various herbs [36,37]. It has versatile applications in medicine, food and pharmaceutical industries because of its unique physiochemical characteristics, such as non-toxicity, biodegradability, abundant availability, and low cost. GA possesses multi-therapeutic protecting capabilities, as well as antioxidant, anti-inflammatory, anticancer, antitumor, antimicrobial, and antidiabetic properties [38–42]. Surface functionalized nanomaterials have demonstrated that attachment of antioxidants results in increased antioxidant activity and bioavailability [43,44]. Previous studies have reported the successful functionalization of GA on silica nanoparticles surface, which was identified as an efficient nanoantioxidant [44,45]. The bimetallic (Ag-Se) nanoparticles functionalized with quercetin and gallic acid were used as antioxidant, antimicrobial, and antitumor agents [46].

Superparamagnetic iron oxide has numerous applications, such as in MRI [19], drug delivery systems [20,21], hyperthermia [23], immunoassay and tissue repair and detoxification [24]. Magnetic nanoparticles loaded with antioxidant enzymes (such as superoxide dismutase (SOD) or catalase (CAT)) have been used as in drug delivery system through magnetic guiding. Magnetically-responsive antioxidant nanocarriers can provide therapeutic guiding of high concentrations of antioxidants to specific locations with elevated levels of ROS [25]. Catalase-loaded magnetic nanoparticles showed rapid cellular uptake and provided increased resistance to oxidative stress damage induced by hydrogen peroxide [2,25]. Magnetic nanoparticles have been used for targeted enzyme therapy, which might be used in the treatment of cardiovascular diseases [25,47] that are related to oxidative damage [2]. Recent studies revealed that iron oxide nanoparticles exhibited antioxidant properties and their activity increased with the decrease in particle size [12].

Biomedical applications need nano-sized particles with high magnetization value and narrow particle size distribution. Furthermore, these nanoparticles require a surface coating which must be biocompatible, nontoxic, and must also allow targeted drug delivery to specific area. Nanoparticles can be stabilized by various protection strategies which could be organic coating, such as poly(ethyleneglycol) [48], polysaccharide [30], dodecanethiol-polymethacrylic acid [21], and chitosan [31], or a coating with an inorganic coating such as silica [44], metal or non-metal, metal oxide or sulphide [32]. This surface coating protects nanomaterials from agglomeration while at the same time functionlizing it [33,34]. The functionalized magnetic nanoparticles can bind to drugs, proteins, enzymes, antibodies, or nucleotides and can be directed to an organ, tissues, or a tumor using an external magnetic field [24,25,47,49].

In this study, we report on IONP functionalized with GA as diverse water-soluble antioxidants which have favorable therapeutic and industrial applications. The resulted IONPs@GA nano-antioxidant has advanced biocompatibility, hydrophilicity, and further synergistic organic-inorganic hybrid antioxidant properties. We investigated the influence of GA in the size-controlled synthesis process and the surface functionalization of Fe_3O_4 nanoparticles by the in situ oxidation-precipitation of ferrous hydroxide method. Prediction of biological activities of GA molecule at IONP surface was performed with the Prediction Activity Spectra of Substances (PASS) training set. Analytical results based on antioxidant and antimicrobial activities confirmed the predictions obtained by the PASS program.

2. Results

2.1. Fourier-Transform Infrared Spectroscopy (FTIR) Analysis

The FTIR spectra of Iron oxide nanoparticles (IONP), In situ functionalized iron oxide nanoparticles IONP@GA1, IONP@GA2 and post-functionalized IONP@GA3 are illustrated by Figure

1a. The peak at 550, 551, 554, and 554 cm^{-1} represent the characteristic Fe-O stretching of for IONP, IONP@GA1, IONP@GA2 and IONP@GA3, respectively [50]. Broad peak at 3100–3200 cm^{-1} refers to OH stretching of phenol. The peak at 1079, 1089, and 1078 cm^{-1} corresponds to Fe-O-C for sample IONP@GA1, IONP@GA2 and IONP@GA3, respectively. Peak at 1633, 1611, and 1630 cm^{-1} confirms the presence of carbonyl group in IONP@GA1, IONP@GA2, and IONP@GA3, respectively.
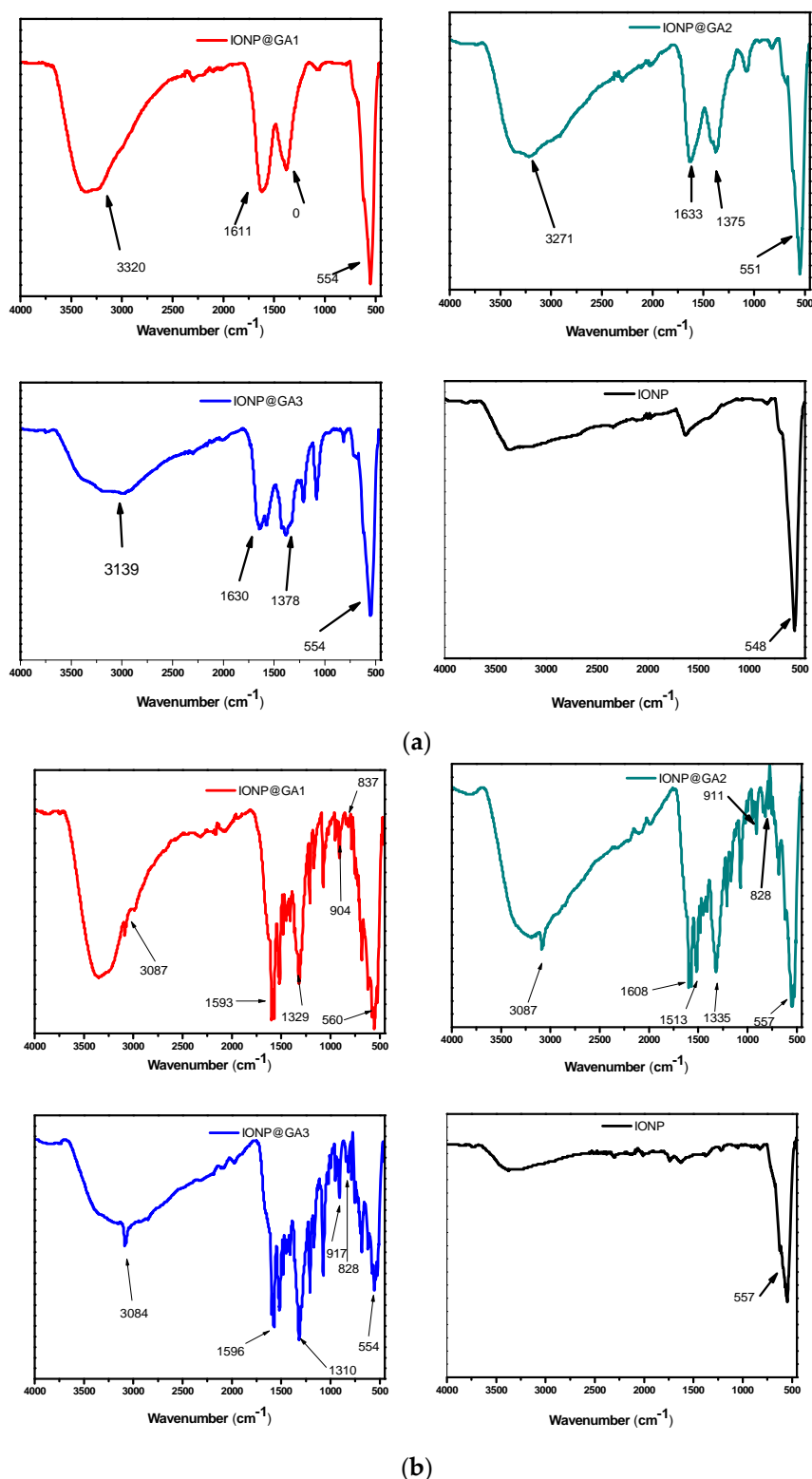

Figure 1. FTIR spectra of (**a**) IONP@GA before DPPH assay (**b**) IONP@GA after DPPH assay.

Further the surface reactivity was ascertained after 2,2-diphenyl-1-picrylhydrazyl (DPPH) assay. Figure 1b shows the FTIR spectra of IONP@GA samples after DPPH assay. IONP@GA samples were mixed with the excess DPPH. The mixture was kept in the dark for 30 min and then washed thrice with ethanol. N-O stretching gave two peaks at 1530, 1310, 1513, 1335, 1530, and 1329 cm^{-1} for IONP@GA3, IONP@GA1, and IONP@GA2, respectively. This confirms the attachment of DPPH radical (ESI, Figure S7) to the surface of IONP@GA. Not a single peak for DPPH radicals was appeared for IONP.

2.2. Raman Spectra

Raman spectra of IONP@GA samples are shown in Figure 2. The structural phase of the synthesized nanoparticles is further supported by Raman spectroscopy that shows the band absorption at 671 cm^{-1} (A1g) is for magnetite [51]. In addition to main band absorption at 671 cm^{-1}, all the samples show peaks at 466 cm^{-1} (T2g) and 348 cm^{-1} (Eg) of magnetite. Moreover, the Raman spectra also confirmed the absence of maghemite (ESI, Figure S8) [52,53].
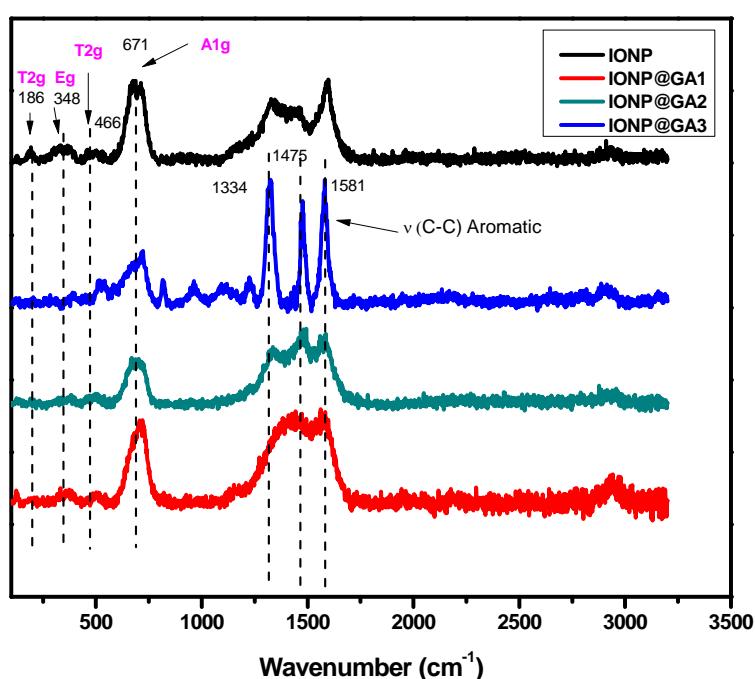

Figure 2. Raman spectra of IONP@GA.

2.3. X-ray Diffraction(XRD) Analysis

The XRD peak patterns of unfunctionalized and functionalized iron oxide nanoparticle are illustrated by Figure 3. XRD reflections shows pure magnetite nanoparticle with cubic inverse spinal structure in all the samples (JCPDS No. 82-1533) [22] ESI, Figure S9. Further, diffraction peaks for magnetite appeared at the 2θ value of 25°, 30°, 43°, 57°, and 63°, correspond to [311], [220], [400], [422] and [440] lattice planes, respectively. The absence of superlattice diffractions at [210], [213] and [300] confirms that maghemite is not present in any sample. Moreover, XRD data confirms that coating did not affect the phase of iron oxide.
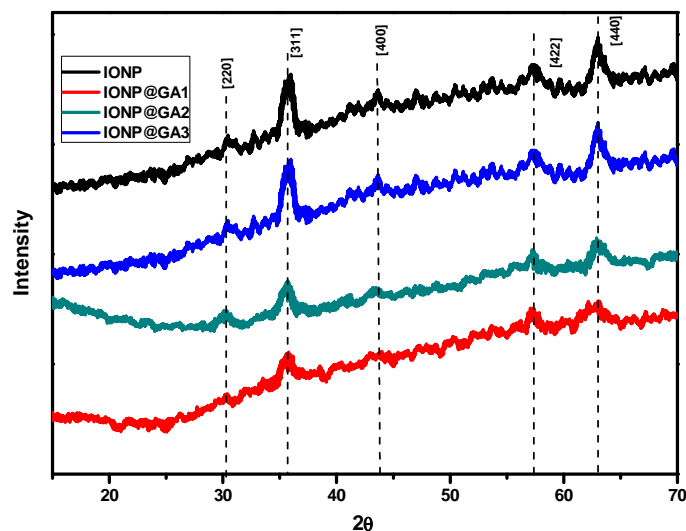
Figure 3. XRD spectra of unfunctionalized and functionalized IONP.

2.4. Morphological Characterization

The morphology of the synthesized IONP@GA was analyzed using High Resolution Transmission Electron Microscopy (HRTEM). Figure 4 shows the HRTEM image with size distribution for GA functionalized magnetite nanoparticles. The average size for IONP@GA1, IONP@GA2, and IONP@GA3 and IONP are 5, 8, 10.8 and 10.0 nm, respectively (Figure 4b,d,f,h). It is clear from the image that the particles have spherical shape with uniform size distribution. Crystal lattice fringe spacing of 0.26 nm, corresponding to the [220] lattice planes in cubic iron oxide nanoparticles [54]. The agglomeration of nanoparticles occurs due to the magnetic behavior of the particles.
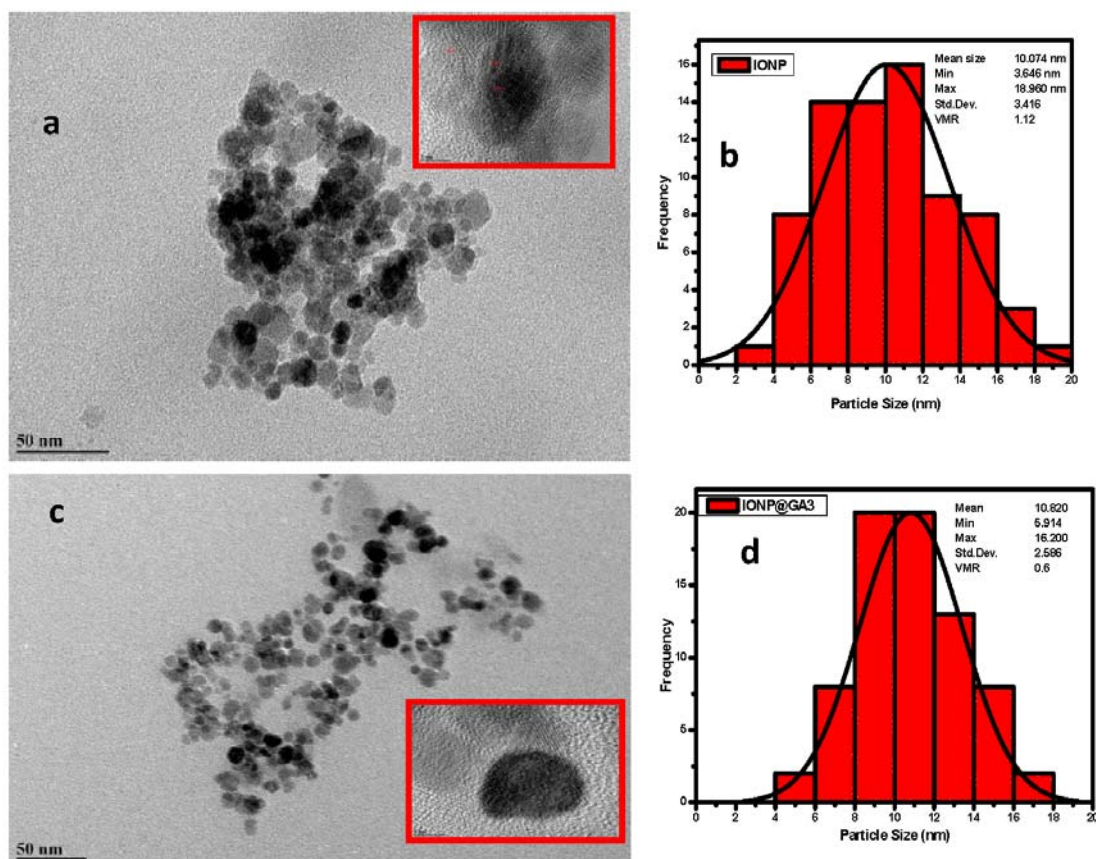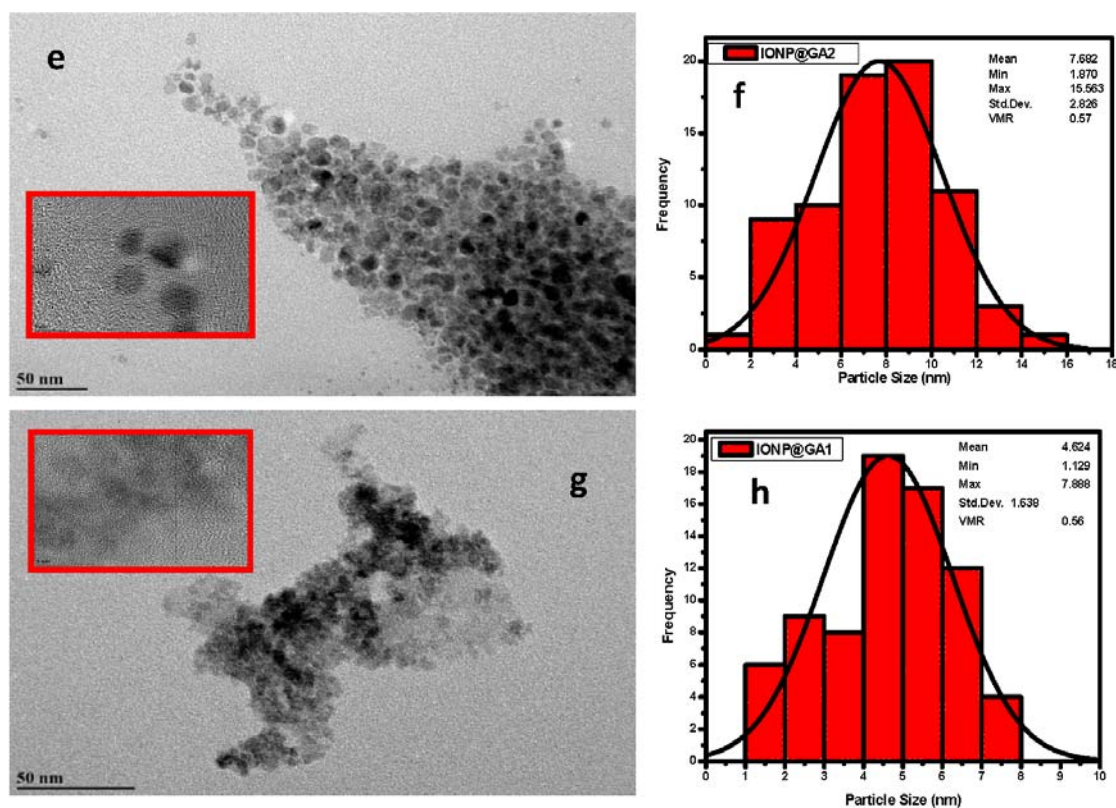
Figure 4. HRTEM images (**a**,**c**,**e**,**g**) and particle size distribution (**b**,**d**,**f**,**h**) of IONP@GA.

The in situ functionalized IONP@GA1 and IONP@GA2 have ultra-small particle size as compared to IONP and post functionalized IONP@GA3 as shown in Figure 4. This reveals that the in-situ functionalization process followed in this study has a strong and successful size-control effect, which is significantly lower than other synthesis routes.

The remarkable size-control effect exerted by GA on in situ-functionalized IONP, can be attributed to iron cations chelate with GA (Figure 5) to form blue-black ferrous/ferric gallate [13,55]. In the same context, GA had minimized the IONP agglomeration, which might be due to either GA bonding site, which strongly coordinates with the IONP surface by forming a monolayer on the IONP surface, which leads to a decrease in magnetic dipole-dipole interaction among the aggregates during formation of nanoparticles and/or the presence of the bulky phenyl group in GA provides sufficient steric hindrance to minimize the IONP agglomeration. Moreover, GA has hydrophilic functional groups, which improves the solubility of IONP in polar solvents and could serve as potential H-bonding sites [56]. Overall, GA has proved an astounding ability to control particle size, solution stability, and hydrophilicity of the IONP nano-antioxidant system.
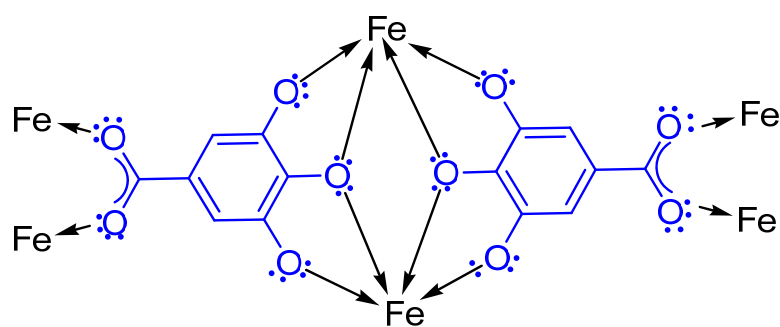
Figure 5. Proposed structure of iron gallate.

2.5. Magnetic Properties

Figure 6 shows the hysteresis loops as a function of the magnetic field at room temperature. The values of 64.19, 60.28, 53.43 and 43.92 emu g^{-1} were given for IONP, IONP@GA2, IONP@GA3, and IONP@GA1, respectively. The magnetic parameters, including saturation magnetization are shown in Table 1. The nanoparticles synthesized here are superparamagnetic with low magnetization values than the bulk magnetite (~92 emu g^{-1}) [57]. Functionalized IONPs showed a decrease in saturation magnetization which was most likely due the decrease in saturation magnetization for functionalized IONPs was due to the presence of more organic contents and impurities on the surface of the magnetic nanoparticles [22,58,59].
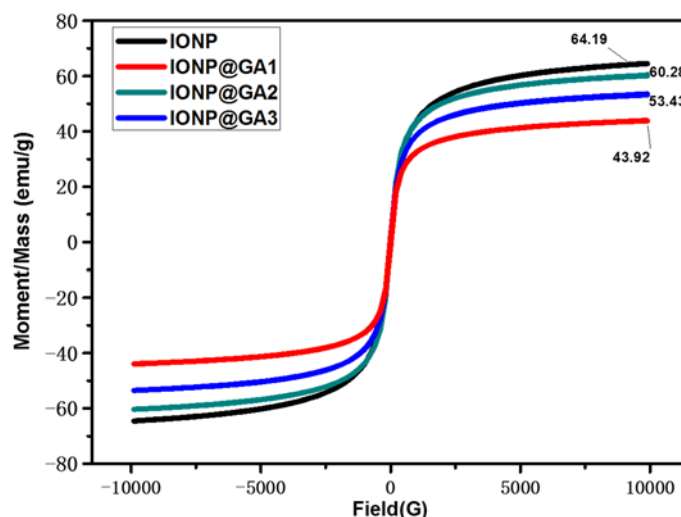
Figure 6. Magnetic hysteresis loops of IONP@GA.

Table 1. Saturation magnetizations of IONPs.

Sample	*Ms* (emu g^{-1})
IONP	64.19
IONP@GA1	43.90
IONP@GA2	60.26
IONP@GA3	53.43

2.6. Energy Dispersive X-ray Spectroscopy (EDX) Analysis

Fe and O signals confirmed the presence of magnetite nanoparticles, while the C signals are derived from the organic matrix as shown in Table 2 (ESI, Figures S1–S4). N signals were also observed in sample IONP@GA1 and IONP@GA2 which might be due to formation of ferrous/ferric gallate during synthesis. The spatial distribution of the iron atoms observed from the mapping images, clearly indicates the uniform distribution of the atoms. Figure 7a–d represents the EDX of IONP@GA1, IONP@GA2, IONP@GA3, and IONP, respectively, after conducting DPPH assay.

Table 2. EDX elemental composition (**A**) Before DPPH assay (**B**) After DPPH assay.

Sample	A				B			
	Fe	O	C	N	Fe	O	C	N
IONP	69.6	39.4	-	-	77.5	21.2	1.3	-
IONP@GA1	62	30.2	7	0.6	62.6	29.5	7.2	0.8
IONP@GA2	65.6	29.1	4.8	0.4	63.7	29.7	6	0.6
IONP@GA3	58.7	30	10.8	-	61.5	26.4	11.7	0.3
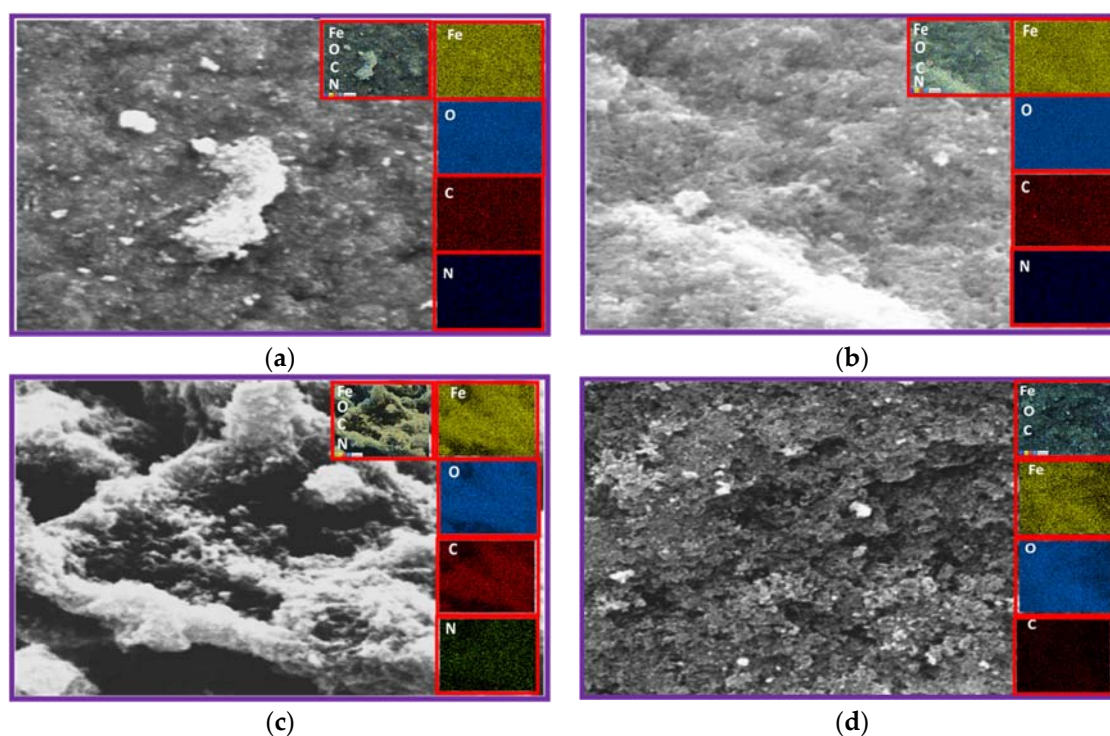
Figure 7. FESEM image (**a**) IONP@GA1 (inset: EDX elemental map of Fe, O, C, and N); (**b**) IONP@GA2 (inset: EDX elemental map of Fe, O, C, and N); (**c**) IONP@GA3 (inset: EDX elemental map of Fe, O, C, and N); and (**d**) IONP (inset: EDX elemental map of Fe, O, C).

The EDX mapping after the DPPH assay, indicates an increase in the percentage of carbon and nitrogen, which could be strongly attributed to attachment of DPPH radicals on the surface of IONP@GA to form IONP@GA-DPPH, which is in agreement with the FTIR results. Nitrogen contents increased from 0% to 0.8%, 0.4% to 0.6%, and 0.6% to 0.3% for IONP@GA1, IONP@GA2, and IONP@GA3 respectively, while carbon contents increased from 7% to 7.2%, 4.8% to 6%, and 10.8% to 11.7% for IONP@GA1, IONP@GA2, and IONP@GA3, respectively. No change in nitrogen contents for unfunctionalized IONP was observed, which indicated that free radicals could not attach to the IONP surface.

2.7. Prediction Activity Spectra of Substances (PASS) of Biological Activity

PASS predictions have been applied to design of new potent free radical inhibitors in phenol series as potential antioxidant drugs [4,60,61]. PASS provides simultaneous predictions over 4000 kinds of biological activity with mean accuracy of 95% [62–65]. The outcome of prediction is available Table 3 as list of activities with appropriate Pa (probability "to be active") to Pi (probability "to be inactive") ratio for GA. It is reasonable that only those types of activities may be revealed by the compound, which Pa > Pi [66]. A portion of the predicted biological activity spectra for the GA is given in Table 3.

Table 3. Predicted biological activity spectra of the GA on the basis of PASS prediction software.

Biological Activity	Pa [a]	Pi [b]
Antioxidant	0.529	0.005
Free Radical Scavenger	0.579	0.007
Lipid Peroxidase Inhibitor	0.554	0.012
Anti-inflammatory	0.560	0.041
Antibacterial	0.420	0.026
Antibacterial, ophthalmic	0.255	0.005
Antifungal	0.255	0.050
Antifungal (Pneumocystis)	0.109	0.003

[a] Probability "to be active"; [b] Probability "to be inactive".

2.8. Antioxidant Activity

The color of the DPPH solution in the presence of the functionalized iron oxide changes gradually from deep violet to pale yellow, which provides the visual monitoring of the antioxidant activity of the nanoparticles. From the UV-VIS absorption curve in Figure 8, it can be inferred that the peak intensity of DPPH is lowering. The free radical scavenging percentage is calculated from the decrease in absorbance at 517 nm. In the DPPH scavenging assay, the IC50 value (Table 4) and the inhibition of stable DPPH free radicals of the compounds were found to be IONP@GA1 (2.7 ± 0.003 mg/mL; 61%), IONP@GA2 (2.2 ± 0.002 mg/mL; 59%) and IONP@GA3 (IC50 1 ± 0.003 mg/mL; 78%) at 10^{-4} M, which are 2–4 fold more than the unfunctionalized IONP (IC50 4.7 ± 0.002 mg/mL; 50%) (Table 4) as a reference in this assay. The DPPH scavenging of four samples was found to be in the order of IONP@GA3 > IONP@GA1 > IONP@GA2 > IONP. The free radical scavenging is most probably due to electron transfer from IONP@GA to free radicals located at the central nitrogen atom of DPPH. Enhanced free radical scavenging for IONP@GA is due to the synergistic effect of IONP and GA.
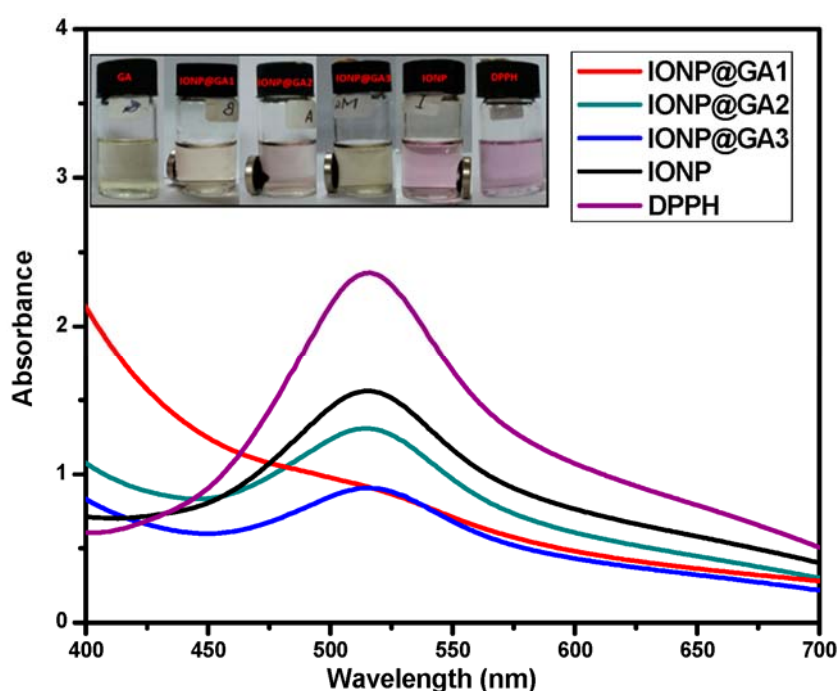

Figure 8. UV-VIS spectra.

Table 4. IC50 of IONP@GA.

Sample		IC50 mg/mL	% Inhibition
IONP@GA3	5 mg	1.00 ± 0.003	78
IONP@GA2	5 mg	2.2 ± 0.002	59
IONP@GA1	5 mg	2.7 ± 0.003	61
IONP	5 mg	4.7 ± 0.002	50

[a] IC50: 50% effective concentration; [b] S.E.M: standard error of the mean.

2.9. Antimicrobial Activity

2.9.1. Antibacterial Activity

Figure 9A shows the results of agar well diffusion test expressed as percentage inhibition of diameter growth (PIDG) of IONP at a concentration of 100 mg/mL. All three types of functionalized IONP@GA showed antibacterial activity on both Gram-positive and -negative strains. However, the

highest growth inhibition percentages were observed upon using IONP@GA3, in which all bacterial strains scored high inhibition values. Thus, revealing its prominent and powerful bactericidal effect.

Generally, results showed a variable IONP@GA antibacterial activity among different bacterial strains. Such trend can be explained based on cell wall composition of each type. Upon administration of IONP@GA, bacterial growth inhibition is believed to occur through the penetration of functionalized IONPs into cells with subsequent cell wall damage by breaking β-1,4-glyosidic bond. Nevertheless, nano-antioxidant IONP@GA compounds were proven to exhibit antibacterial activity on both bacterial strains.
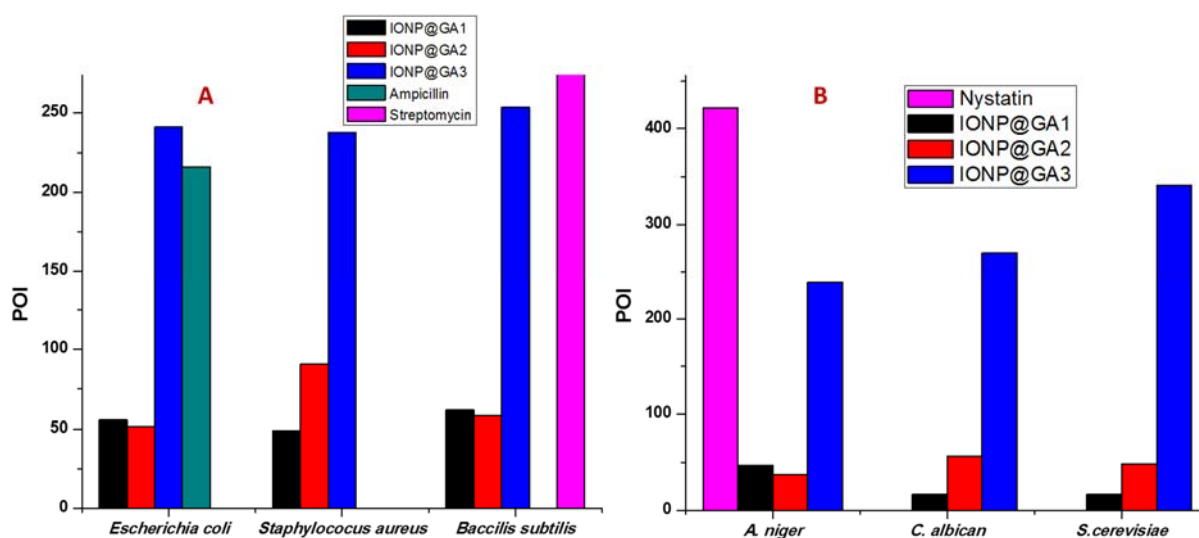
Figure 9. Percentage of inhibition (POI) of (**A**) bacterial growth and (**B**) mycelia growth of fungi, after treatment with IONP@GA.

2.9.2. Antifungal Activity

The antifungal activity of IONP@GA against *Aspergillus niger*, *Candida albicans*, and *Saccharomyces cerevisiae* was investigated using the well diffusion method. Results, as presented in Figure 9B, show a potent antifungal activity of tested compounds among all fungi strains used. The highest percentage of inhibition (POI) was obtained by utilizing IONP@GA3 compound. Together with its antibacterial activity, these results confirm the higher antimicrobial activity of IONP@GA3 compared to other functionalized IONP compounds. The mechanism responsible for antifungal activity seen, can be assumed to involve the attachment of nanoparticles to the respiratory sequence, which leads to cell death [67].

With reference to the above discussed results, the synthesized nano-antioxidant IONP@GA in this study had proven to own strong antimicrobial properties, that potentiate various biomedical applications. Yet, the astonishing antioxidant activity of IONP@GA compounds may find further applications in industrial fields. Herein, we propose a potential application of nanomagnetite in industries as illustrated in Figure 10. We propose that controlling the size and antioxidant activity is a promising method for improving industrial based materials. These magnetic nanoantioxidants have many advantages over conventional antioxidants. In addition to the GA functional moiety that enables less toxic, biocompatible coating with fine size-control, the mixture of IONP@GA and toxic materials (IONP@GA-ROS) formed during the reaction of nanomagnetite with ROS can be easily removed from the system by a magnet and can be recycled.
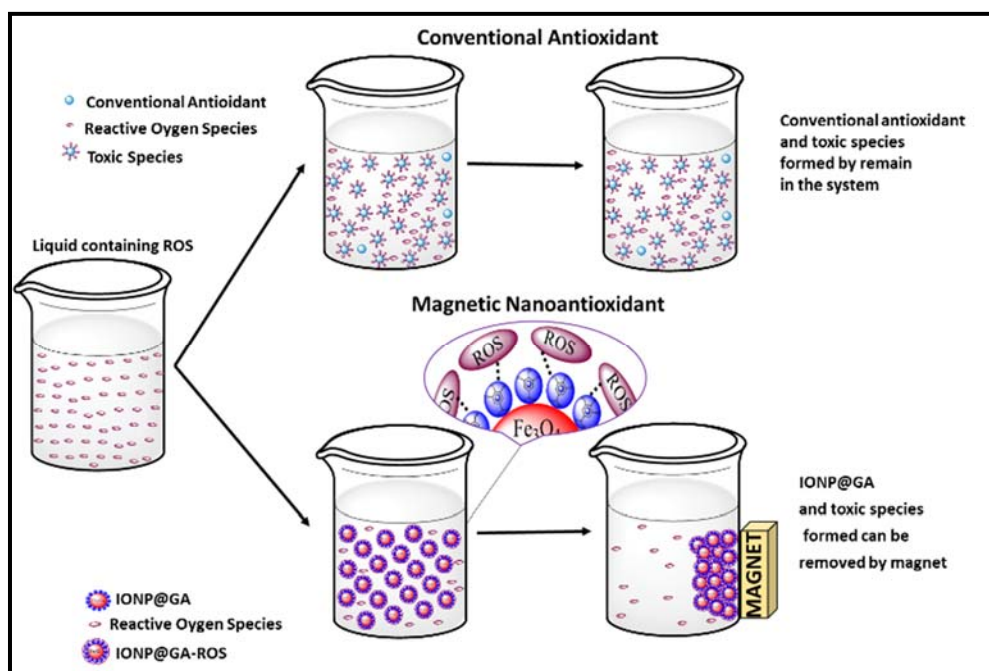
Figure 10. Proposed potential applications of IONP@GA in industry.

3. Discussion

GA functionalized organic nanomagnetites have been successfully synthesized via in situ and post-functionalization techniques. The average particle size is 5 and 8 nm for in situ-functionalized nanomagnetie IONP@GA1 and IONP@GA2, respectively, while it is 11 nm for post-functionalized IONP@GA3. The particle size fall in order of IONP@GA3 > IONP > IONP@GA2 > IONP@GA1. Addition of GA during in-situ synthesis had controlled the particle size of IONP, thus efficiently overcoming a critical obstacle in nano-antioxidant synthesis. PASS-predicted antioxidant values and other biological activities for the GA indicated that the GA-functionalized IONP surface could be likely to reveal these activities, in addition to the iron oxide activities and its biocompatibility as multi-purpose tools for guided drug delivery and bioimaging. The DPPH scavenging of the four samples is found to be in the order of IONP@GA3 > IONP@GA1 > IONP@GA2 > IONP. The in situ and post functionalization methods successfully improved the free radical scavenging of IONP to be more than 2–4 fold. The present investigation highlights the synergistic effect of the magnetite and GA, which leads to the enhancement of the free radical scavenging capacity of IONP@GA. The synthesized IONPs@GA samples are hydrophilic and exhibited greater antioxidant activity and degraded the DPPH radicals efficiently. FTIR and EDX techniques confirmed that IONP@GA is scavenged the DPPH radicals and yielding IONP@GA-DPPH composite suggesting that free radicals can be easily removed from the system by magnet and can be recycled. Finally, IONP@GA showed potential antimicrobial activity (antibacterial and antifungal) effects on strains tested, probably through the destruction of membrane integrity; therefore, it was concluded that IONP@GA has considerable antimicrobial activity, which is promising for further clinical applications. The methodology used here can be employed for synthesizing organic nanocompounds with other antioxidants that are magnetically separable, efficient, low cost and may have potential applications in polymer, cosmetics, biomedical and food industry.

4. Materials and Methods

4.1. Materials

Ferrous chloride tetrahydrate ($FeCl_2 \cdot 4H_2O$, Merck, Mendota Heights, MN, USA), ferric chloride hexahydrate ($FeCl_3 \cdot 6H_2O$, Sigma ≥ 97%, (Saint Louis, MO, USA)), Gallic acid (R and M) and ammonia

solution (R and M, 28%) (Shanghai, China) were used as received without further purification. Analytical grade reagents were used during all experiments. The shape and size of samples were analyzed using a (JEOL JEM-2100F, Tokyo, Japan). Phase identification and crystallinity of the magnetite samples were determined using a PANalytical X-ray diffractometer (model EMPYREAN, Almelo, The Netherlands) where Cu-Kα (λ = 1.54060 Å) radiation was used. The spectra has been recorded for 2θ ranging from 10.00 to 90.00. FTIR of the samples was recorded using a Spectrum 400 (PerkinElmer, Boston, MA, USA). EDX was studied using EDX (INCA Energy 200 (Oxford Inst.), Hillsboro, OR, USA). The percentage composition was determined using the surface area method. The Raman spectra were obtained from Renishaw inVia Raman (Gloucestershire, UK) by using a 514 nm argon gas laser. The magnetism hysteresis loop was obtained from a Lake Shore vibrational sample magnetometer (VSM) (Westerville, OH, USA) at room temperature in a magnetic field range of −10 to +10 kOe.

4.2. Synthesis of IONP

Ferrous chloride and ferric chloride with a molar ratio of 1:1.5 was dissolved in 100 mL deionized water. Ammonium hydroxide solution (3.0 M) was added 5.0 mL min^{-1} into the solution at a stirring speed of 600 rpm to reach a final pH 11. The reaction was carried out at 80 °C under an oxidizing environment and stirring was continued for another 90 min. The resultant black precipitate was isolated by magnetic decantation. The precipitate was rinsed with deionized water and ethanol. After that, it was freeze dried.

4.2.1. In Situ Functionalization

Synthesis of Organic IONP@GA1

Ferrous chloride and ferric chloride with a molar ratio of 1:1.5 was dissolved into 100 mL deionized water, followed by the addition of 1 g GA. 3.0 M of ammonium hydroxide solution was added 5.0 mL min^{-1} into the solution at 600 rpm stirring speed to reach a final pH 11. The reaction was conducted at 80 °C under oxidizing environment with continued stirring for another 90 min. The resultant black precipitate was isolated by magnetic decantation. Lastly, the precipitate was rinsed with deionized water and ethanol, then freeze-dried.

Synthesis of Organic IONP@GA2

Ferrous chloride and ferric chloride with a molar ratio of 1:1.5 was dissolved in 100 mL deionized water. Ammonium hydroxide solution (3.0 M) was added at a speed of 5.0 mL min^{-1} into the solution at a stirring speed of 600 rpm to reach a final volume of 100 mL. One gram of GA was added to the reaction mixture. The reaction was carried out at 80 °C under an oxidizing environment with continued stirring for another 90 min. The resultant black precipitate was isolated by magnetic decantation. Finally, the precipitate was rinsed with deionized water and ethanol, then freeze-dried.

4.2.2. Post-Functionalization

Synthesis of IONP@GA3

One gram of GA was mixed with the IONP and was kept under stirring for 24 h. The precipitate was rinsed with deionized water and ethanol, then freeze-dried.

4.2.3. Antioxidant Activity

Various chemical based assays have been used to determine antioxidant activities. Based on the reaction involved, these assays can be classified into two main types. Hydrogen atom transfer and electron transfer. In this present work, the DPPH assay involving electron transfer was selected to study the antioxidant activity of functionalized magnetite nanoparticles [45]. The antioxidant activity was determined by using a standard DPPH method with some modification [44,45]. Sample stock

suspensions in methanol (300 μL) and 1 mL of methanolic solution of DPPH (0.2 mM) were mixed in a 1 cm quartz cuvettes. Absorbance measurements were taken after 30 min. The decrease in absorbance at 517 nm was observed continuously. All the experiments were duplicated. All the measurements were taken within exactly 30 min after mixing the sample with DPPH solution. The radical scavenging activity was calculated using Equation (1):

$$\text{Percentage of Inhibition (\%)} = \frac{(Ac - As)}{Ac} \times 100 \tag{1}$$

In which As = the absorbance of the compounds/positive control and Ac = the absorbance of the control (DPPH solution). To determine the concentration required to achieve 50% inhibition (IC_{50}) of the DPPH radical; the percentage of DPPH inhibition for each compound was plotted against different concentrations.

4.2.4. Antimicrobial Activity

Determination of Antibacterial Activity

The antibacterial activities of the IONP@GA were estimated using the agar well diffusion method [68]. Precultures of *Staphylococcus aureus*, *Bacillus substilis*, and *Escherichia coli* were spread on the surface of nutrient agar (NA) agar and wells (diameter = 6 mm) were filled with 100 μL of the test samples (100 mg/mL) and incubated at 37 °C for 24 h. Sterile distilled water was used as a negative control. Positive controls used were streptomycin 100 mg/disc and ampicillin 100 mg/mL for Gram-positive and Gram-negative bacteria, respectively. The formation of the halo (inhibition) zone and the diameter of inhibition zones were determined to evaluate the antibacterial properties.

Determination of Antifungal Properties

For antifungal properties, all IONP@GA types were tested against *Aspergillus niger*, a filamentous fungus (multicellular); *Saccharomyces cerevisiae*, a yeast (unicellular); and *Candida albican*, a yeast using the well diffusion method. PDA agar plates were inoculated with fungal strains under aseptic conditions and wells (diameter = 6 mm) were filled with 100 μL of the test samples (100 mg/mL) and incubated at 25 °C for 48 h. Sterile distilled water was used as negative control. The positive control used was nystatin at 100 mg/mL. The percentage of inhibition (POI) of mycelia growth was calculated using Equation (2):

$$POI = \frac{R1 - R2}{R1} \times 100 \tag{2}$$

where

$R1$ = radius of the pathogen away from the antagonist.
$R2$ = radius of the pathogen towards the antagonist.

References

1. Patrick-Iwuanyanwu, K.; Onyeike, E.; Adhikari, A. Isolation, identification and characterization of gallic acid derivatives from leaves of tapinanthus bangwensis. *J. Nat. Prod.* **2014**, *7*, 14–19.

2. Erica, S.; Daniel, A.; Silvana, A. Artificial nanoparticle antioxidants. In *Oxidative stress: Diagnostics, prevention, and therapy*, American Chemical Society: Washington, DC, USA,, 2011; Vol. 1083, pp 235–253.

3. Urso, M.L.; Clarkson, P.M. Oxidative stress, exercise, and antioxidant supplementation. *Toxicol.* **2003**, *189*, 41–54.

4. Yehye, W.A.; Rahman, N.A.; Ariffin, A.; Abd Hamid, S.B.; Alhadi, A.A.; Kadir, F.A.; Yaeghoobi, M. Understanding the chemistry behind the antioxidant activities of butylated hydroxytoluene (bht): A review. *Eur. J. Med. Chem.* **2015**, *101*, 295–312.

5. Armstrong, D.; Bharali, D.J.; Armstrong, D.; Bharali, D. Oxidative stress and nanotechnology. *Methods and Protocols* **2013**, *1028*.

6. Sandhir, R.; Yadav, A.; Sunkaria, A.; Singhal, N. Nano-antioxidants: An emerging strategy for intervention against neurodegenerative conditions. *Neurochem. Int.* **2015**, *89*, 209–226.

7. Esumi, K.; Takei, N.; Yoshimura, T. Antioxidant-potentiality of gold–chitosan nanocomposites. *Colloids Surf. B. Biointerfaces* **2003**, *32*, 117–123.

8. BarathManiKanth, S.; Kalishwaralal, K.; Sriram, M.; Pandian, S.R.K.; Youn, H.-s.; Eom, S.; Gurunathan, S. Anti-oxidant effect of gold nanoparticles restrains hyperglycemic conditions in diabetic mice. *J. Nanobiotechnology* **2010**, *8*, 16–16.

9. Kim, J.; Takahashi, M.; Shimizu, T.; Shirasawa, T.; Kajita, M.; Kanayama, A.; Miyamoto, Y. Effects of a potent antioxidant, platinum nanoparticle, on the lifespan of caenorhabditis elegans. *Mech. Ageing Dev.* **2008**, *129*, 322–331.

10. Kajita, M.; Hikosaka, K.; Iitsuka, M.; Kanayama, A.; Toshima, N.; Miyamoto, Y. Platinum nanoparticle is a useful scavenger of superoxide anion and hydrogen peroxide. *Free Radic. Res.* **2007**, *41*, 615–626.

11. Moglianetti, M.; De Luca, E.; Pedone, D.; Marotta, R.; Catelani, T.; Sartori, B.; Amenitsch, H.; Retta, S.F.; Pompa, P.P. Platinum nanozymes recover cellular ros homeostasis in an oxidative stress-mediated disease model. *Nanoscale* **2016**, *8*, 3739–3752.

12. Paul, S.; Saikia, J.; Samdarshi, S.; Konwar, B. Investigation of antioxidant property of iron oxide particlesby 1'-1' diphenylpicryl-hydrazyle (dpph) method. *J. Magn. Magn. Mater.* **2009**, *321*, 3621–3623.

13. Toth, I.Y.; Szekeres, M.; Turcu, R.; Saringer, S.; Illes, E.; Nesztor, D.; Tombacz, E. Mechanism of in situ surface polymerization of gallic acid in an environmental-inspired preparation of carboxylated core-shell magnetite nanoparticles. *Langmuir* **2014**, *30*, 15451–15461.

14. Szekeres, M.; Toth, I.Y.; Illes, E.; Hajdu, A.; Zupko, I.; Farkas, K.; Oszlanczi, G.; Tiszlavicz, L.; Tombacz, E. Chemical and colloidal stability of carboxylated core-shell magnetite nanoparticles designed for biomedical applications. *Int. J. Mol. Sci.* **2013**, *14*, 14550–14574, 14525 pp.

15. Saikia, J.P.; Paul, S.; Konwar, B.K.; Samdarshi, S.K. Nickel oxide nanoparticles: A novel antioxidant. *Colloids Surf. B. Biointerfaces* **2010**, *78*, 146–148.

16. Niu, J.; Wang, K.; Kolattukudy, P.E. Cerium oxide nanoparticles inhibits oxidative stress and nuclear factor-κb activation in h9c2 cardiomyocytes exposed to cigarette smoke extract. *J. Pharmacol. Exp. Ther.* **2011**, *338*, 53–61.

17. Kim, C.K.; Kim, T.; Choi, I.-Y.; Soh, M.; Kim, D.; Kim, Y.-J.; Jang, H.; Yang, H.-S.; Kim, J.Y.; Park, H.-K., et al. Ceria nanoparticles that can protect against ischemic stroke. *Angew. Chem., Int. Ed.* **2012**, *51*, 11039–11043.

18. Schubert, D.; Dargusch, R.; Raitano, J.; Chan, S.-W. Cerium and yttrium oxide nanoparticles are neuroprotective. *Biochem. Biophys. Res. Commun.* **2006**, *342*, 86–91.

19. Zhu, J.; Wang, J.; Wang, X.; Zhu, J.; Yang, Y.; Tian, J.; Cui, W.; Ge, C.; Li, Y.; Pan, Y., et al. Facile synthesis of magnetic core-shell nanocomposites for mri and ct bimodal imaging. *J. Mater. Chem. B* **2015**, *3*, 6905–6910.

20. Tudisco, C.; Cambria, M.T.; Sinatra, F.; Bertani, F.; Alba, A.; Giuffrida, A.E.; Saccone, S.; Fantechi, E.; Innocenti, C.; Sangregorio, C., et al. Multifunctional magnetic nanoparticles for enhanced intracellular drug transport. *J. Mater. Chem. B* **2015**, *3*, 4134–4145.

21. Majeed, M.I.; Lu, Q.; Yan, W.; Li, Z.; Hussain, I.; Tahir, M.N.; Tremel, W.; Tan, B. Highly water-soluble magnetic iron oxide (fe3o4) nanoparticles for drug delivery: Enhanced in vitro therapeutic efficacy of doxorubicin and mion conjugates. *J. Mater. Chem. B* **2013**, *1*, 2874–2884.

22. Dorniani, D.; Hussein, M.Z.B.; Kura, A.U.; Fakurazi, S.; Shaari, A.H.; Ahmad, Z. Preparation of fe3o4 magnetic nanoparticles coated with gallic acid for drug delivery. *Int. J. Nanomedicine* **2012**, *7*, 5745–5756.

23. Blanco-Andujar, C.; Ortega, D.; Southern, P.; Pankhurst, Q.A.; Thanh, N.T. High performance multi-core iron oxide nanoparticles for magnetic hyperthermia: Microwave synthesis, and the role of core-to-core interactions. *Nanoscale* **2015**, *7*, 1768–1775.

24. Gupta, A.K.; Gupta, M. Synthesis and surface engineering of iron oxide nanoparticles for biomedical applications. *Biomaterials* **2005**, *26*, 3995–4021.

25. Chorny, M.; Hood, E.; Levy, R.J.; Muzykantov, V.R. Endothelial delivery of antioxidant enzymes loaded into non-polymeric magnetic nanoparticles. *J. Control. Release* **2010**, *146*, 144–151.

26. Verma, A.K. Anti-oxidant activities of biopolymeric nanoparticles: Boon or bane! *J. Pharm. Res.* **2014**, *8*, 871–876.

27. Samuel, E.L.G.; Duong, M.T.; Bitner, B.R.; Marcano, D.C.; Tour, J.M.; Kent, T.A. Hydrophilic carbon clusters as therapeutic, high-capacity antioxidants. *Trends Biotechnol.* **2014**, *32*, 501–505.

28. Sharpe, E.; Andreescu, D.; Andreescu, S. Artificial nanoparticle antioxidants. *ACS Symp. Ser.* **2011**, *1083*, 235–253.

29. Cîrcu, M.; Nan, A.; Borodi, G.; Liebscher, J.; Turcu, R. Refinement of magnetite nanoparticles by coating with organic stabilizers. *Nanomaterials* **2016**, *6*, 228.

30. Santiago-Rodriguez, L.; Lafontaine, M.M.; Castro, C.; Mendez-Vega, J.; Latorre-Esteves, M.; Juan, E.J.; Mora, E.; Torres-Lugo, M.; Rinaldi, C. Synthesis, stability, cellular uptake, and blood circulation time of carboxymethyl-inulin coated magnetic nanoparticles. *J. Mater. Chem. B* **2013**, *1*, 2807–2817.

31. Nasirimoghaddam, S.; Zeinali, S.; Sabbaghi, S. Chitosan coated magnetic nanoparticles as nano-adsorbent for efficient removal of mercury contents from industrial aqueous and oily samples. *J. Ind. Eng. Chem.* **2015**, *27*, 79–87.

32. Tancredi, P.; Botasini, S.; Moscoso-Londoño, O.; Méndez, E.; Socolovsky, L. Polymer-assisted size control of water-dispersible iron oxide nanoparticles in range between 15 and 100 nm. *Colloids Surf. Physicochem. Eng. Aspects* **2015**, *464*, 46–51.

33. Bhattacharya, K.; Gogoi, B.; Buragohain, A.K.; Deb, P. Fe2o3/c nanocomposites having distinctive antioxidant activity and hemolysis prevention efficiency. *Mater. Sci. Eng., C* **2014**, *42*, 595–600.

34. Sodipo, B.K.; Abdul Aziz, A. Non-seeded synthesis and characterization of superparamagnetic iron oxide nanoparticles incorporated into silica nanoparticles via ultrasound. *Ultrason. Sonochem.* **2015**, *23*, 354–359.

35. Lam, T.; Avti, P.; Pouliot, P.; Maafi, F.; Tardif, J.-C.; Rhéaume, É.; Lesage, F.; Kakkar, A. Fabricating water dispersible superparamagnetic iron oxide nanoparticles for biomedical applications through ligand exchange and direct conjugation. *Nanomaterials* **2016**, *6*, 100.

36. Prakash, O.; Singh, R.M.; Mathur, S.C.; Singh, G.N. Quantification of gallic acid by hplc and antioxidant activity of amla fruits. *J. Pharm. Res.* **2007**, *6*, 161–162.

37. Li, L.; Ng, T.B.; Gao, W.; Li, W.; Fu, M.; Niu, S.M.; Zhao, L.; Chen, R.R.; Liu, F. Antioxidant activity of gallic acid from rose flowers in senescence accelerated mice. *Life Sci.* **2005**, *77*, 230–240.

38. Stanely Mainzen Prince, P.; Kumar, M.R.; Selvakumari, C.J. Effects of gallic acid on brain lipid peroxide and lipid metabolism in streptozotocin-induced diabetic wistar rats. *J. Biochem. Mol. Toxicol.* **2010**, *25*, 101–107.

39. Adefegha, S.A.; Oboh, G.; Ejakpovi, I.I.; Oyeleye, S.I. Antioxidant and antidiabetic effects of gallic and protocatechuic acids: A structure-function perspective. *Comp. Clin Pathol* **2015**, *24*, 1579–1585.

40. Locatelli, C.; Filippin-Monteiro, F.B.; Centa, A.; Creczinsky-Pasa, T.B. *Antioxidant, antitumoral and anti-inflammatory activities of gallic acid*. Nova Science Publishers: New York, 2013; Vol. Handbook on gallic acid: natural occurrences, antioxidant properties and health implications.

41. Seo, D.-J.; Lee, H.-B.; Kim, I.-S.; Kim, K.-Y.; Park, R.-D.; Jung, W.-J. Antifungal activity of gallic acid purified from terminalia nigrovenulosa bark against fusarium solani. *Microb. Pathog.* **2013**, *56*, 8–15.

42. Akiyama, H.; Fujii, K.; Yamasaki, O.; Oono, T.; Iwatsuki, K. Antibacterial action of several tannins against staphylococcus aureus. *Journal of antimicrobial chemotherapy* **2001**, *48*, 487–491.

43. Kojima, N.; Shiraishi, Y.; Hisamatsu, F.; Miyamoto, A.; Kajita, M. Antioxidant for cosmetic, external application medicine, and food and drink. JP2008156440A, 2008.

44. Deligiannakis, Y.; Sotiriou, G.A.; Pratsinis, S.E. Antioxidant and antiradical sio2 nanoparticles covalently functionalized with gallic acid. *ACS Appl. Mater. Interfaces* **2012**, *4*, 6609–6617.

45. Sotiriou, G.A.; Blattmann, C.O.; Deligiannakis, Y. Nanoantioxidant-driven plasmon enhanced proton-coupled electron transfer. *Nanoscale* **2016**, *8.2*, 796–803.

46. Mittal, A.K.; Kumar, S.; Banerjee, U.C. Quercetin and gallic acid mediated synthesis of bimetallic (silver and selenium) nanoparticles and their antitumor and antimicrobial potential. *J. Colloid Interface Sci.* **2014**, *431*, 194–199.

47. Lacramioara, L.; Diaconu, A.; Butnaru, M.; Verestiuc, L. Biocompatible spions with superoxid dismutase/catalase immobilized for cardiovascular applications. In *3rd international conference on nanotechnologies and biomedical engineering*, Sontea, V.; Tiginyanu, I., Eds. Springer Singapore: 2016; Vol. 55, pp 323–326.

48. Li, Y.; Lin, R.; Wang, L.; Huang, J.; Wu, H.; Cheng, G.; Zhou, Z.; MacDonald, T.; Yang, L.; Mao, H. Peg-b-age polymer coated magnetic nanoparticle probes with facile functionalization and anti-fouling properties for reducing non-specific uptake and improving biomarker targeting. *J. Mater. Chem. B* **2015**, *3*, 3591–3603.

49. Laurent, S.; Forge, D.; Port, M.; Roch, A.; Robic, C.; Vander Elst, L.; Muller, R.N. Magnetic iron oxide nanoparticles: Synthesis, stabilization, vectorization, physicochemical characterizations, and biological applications. *Chem. Rev.* **2008**, *108*, 2064–2110.

50. Szekeres, M.; Illés, E.; Janko, C.; Farkas, K.; Tóth, I.Y.; Nesztor, D.; Zupkó, I.; Földesi, I.; Alexiou, C.; Tombácz, E. Hemocompatibility and biomedical potential of poly(gallic acid) coated iron oxide nanoparticles for theranostic use. *J. Nanomed. Nanotechnol.* **2015**, *6*.

51. De Faria, D.; Venâncio Silva, S.; De Oliveira, M. Raman microspectroscopy of some iron oxides and oxyhydroxides. *J. Raman Spectrosc.* **1997**, *28*, 873–878.

52. Shebanova, O.N.; Lazor, P. Raman study of magnetite (fe3o4): Laser-induced thermal effects and oxidation. *J. Raman Spectrosc.* **2003**, *34*, 845–852.

53. Francisco, M.; Teresa, C.; María, C.; Ramón, P.; Rolando, R.; Pedro, F.; José María, S.; Eduardo, E.; Carmen, M. Synthesis and characterization of monodisperse magnetite hollow microspheres. *Soft Nanosci. Lett.* **2011**, *1*, 25–32

54. Iyengar, S.J.; Joy, M.; Ghosh, C.K.; Dey, S.; Kotnala, R.K.; Ghosh, S. Magnetic, x-ray and mossbauer studies on magnetite/maghemite core-shell nanostructures fabricated through an aqueous route. *RSC Adv.* **2014**, *4*, 64919–64929.

55. Krekel, C. The chemistry of historical iron gall inks: Understanding the chemistry of writing inks used to prepare historical documents. *Int. J. forensic document examiners* **1999**, *5*, 54–58.

56. Wang, X.; Tilley, R.D.; Watkins, J.J. Simple ligand exchange reactions enabling excellent dispersibility and stability of magnetic nanoparticles in polar organic, aromatic, and protic solvents. *Langmuir* **2014**, *30*, 1514–1521.

57. Cornell, R.M.; Schwertmann, U. *The iron oxides: Structure, properties, reactions, occurrences and uses*. John Wiley & Sons: Hoboken, NJ, USA,, 2006.

58. Ma, H.-l.; Qi, X.-r.; Maitani, Y.; Nagai, T. Preparation and characterization of superparamagnetic iron oxide nanoparticles stabilized by alginate. *Int. J. Pharm.* **2007**, *333*, 177–186.

59. Dorniani, D.; Bin, H.M.Z.; Kura, A.U.; Fakurazi, S.; Hussein-Al-Ali, S.H.; Shaari, A.H.; Ahmad, Z. In vitro sustained release study of gallic acid coated with magnetite-peg and magnetite-pva for drug delivery system. *Scientific World J.* **2014**, 1–11.

60. Kareem, H.S.; Ariffin, A.; Nordin, N.; Heidelberg, T.; Abdul-Aziz, A.; Kong, K.W.; Yehye, W.A. Correlation of antioxidant activities with theoretical studies for new hydrazone compounds bearing a 3, 4, 5-trimethoxy benzyl moiety. *Eur. J. Med. Chem.* **2015**, *103*, 497–505.

61. Poroikov, V.V.; Filimonov, D.A.; Ihlenfeldt, W.-D.; Gloriozova, T.A.; Lagunin, A.A.; Borodina, Y.V.; Stepanchikova, A.V.; Nicklaus, M.C. Pass biological activity spectrum predictions in the enhanced open nci database browser. *J. Chem. Inf. Comput. Sci.* **2003**, *43*, 228–236.

62. Kadir, F.A.; Kassim, N.M.; Abdulla, M.A.; Yehye, W.A. Pass-predicted vitex negundo activity: Antioxidant and antiproliferative properties on human hepatoma cells-an in vitro study. *BMC Complement. Altern. Med.* **2013**, *13*, 1–13.

63. Stepanchikova, A.; Lagunin, A.; Filimonov, D.; Poroikov, V. Prediction of biological activity spectra for substances: Evaluation on the diverse sets of drug-like structures. *Curr. Med. Chem.* **2003**, *10*, 225–233.

64. Anzali, S.; Barnickel, G.; Cezanne, B.; Krug, M.; Filimonov, D.; Poroikov, V. Discriminating between drugs and nondrugs by prediction of activity spectra for substances (pass). *J. Med. Chem.* **2001**, *44*, 2432–2437.

65. Kadir, F.A.; Kassim, N.M.; Abdulla, M.A.; Kamalidehghan, B.; Ahmadipour, F.; Yehye, W.A. Pass-predicted hepatoprotective activity of caesalpinia sappan in thioacetamide-induced liver fibrosis in rats. *The Scientific World J.* **2014**, 1–12.

66. PharmaExpert. http://www.pharmaexpert.ru/passonline/ (4 April 2015),

67. Rudramurthy, G.R.; Swamy, M.K.; Sinniah, U.R.; Ghasemzadeh, A. Nanoparticles: Alternatives against drug-resistant pathogenic microbes. *Molecules* **2016**, *21*, 836.

68. Sahu, N.; Soni, D.; Chandrashekhar, B.; Sarangi, B.K.; Satpute, D.; Pandey, R.A. Synthesis and characterization of silver nanoparticles using cynodon dactylon leaves and assessment of their antibacterial activity. *Bioprocess. Biosystems Eng.* **2013**, *36*, 999–1004.